A Method for Assessing the Importance of Body Force on Flow Boiling CHF

Hui Zhang

Issam Mudawar
e-mail: mudawar@ecn.purdue.edu

Boiling and Two-phase Flow Laboratory,
School of Mechanical Engineering,
Purdue University,
West Lafayette, IN 47907, USA

Mohammad M. Hasan
NASA Glenn Research Center,
21000 Brookpark Road,
Cleveland, OH 44135, USA

Experiments were performed to examine the effects of body force on flow boiling CHF. FC-72 was boiled along one wall of a transparent rectangular flow channel that permitted photographic study of the vapor-liquid interface just prior to CHF. High-speed video imaging techniques were used to identify dominant CHF mechanisms corresponding to different flow orientations and liquid velocities. Six different CHF regimes were identified: Wavy Vapor Layer, Pool Boiling, Stratification, Vapor Counterflow, Vapor Stagnation, and Separated Concurrent Vapor Flow. CHF showed significant sensitivity to orientation for flow velocities below 0.2 m/s, where extremely low CHF values where measured, especially with downward-facing heated wall and downflow orientations. High flow velocities dampened the effects of orientation considerably. The CHF data were used to assess the suitability of previous CHF models and correlations. It is shown the Interfacial Lift-off Model is very effective at predicting CHF for high velocities at all orientations. The flooding limit, on the other hand, is useful at estimating CHF at low velocities and for downflow orientations. A new method consisting of three dimensionless criteria is developed to determine the minimum flow velocity required to overcome body force effects on near-saturated flow boiling CHF. [DOI: 10.1115/1.1651532]

Keywords: Boiling, Channel Flow, Heat Transfer, Microgravity, Phase Change

1 Introduction

The vast majority of flow boiling critical heat flux (CHF) studies in the heat transfer literature concern vertical upflow. This is not surprising given this orientation provides the greatest flow stability, with the buoyancy force aiding in vapor removal in the same direction as the liquid flow. Numerous horizontal flow CHF studies have also been published, albeit to a much lesser degree than vertical upflow.

For all orientations other than vertical upflow, buoyancy can greatly complicate both the vapor coalescence at the heated wall, including the CHF mechanism itself, and the vapor removal along the flow channel. The role of buoyancy becomes even more complex where only one side of the flow channel is heated. Orientations associated with upward moving fluid and an upward-facing heated wall are generally advantageous because these orientations capitalize upon buoyancy forces to both remove vapor from the wall and expel it axially in the direction of fluid flow. The opposite is true for a downward moving fluid and a downward-facing heated wall. Here, buoyancy causes accumulation of the vapor along the wall, as well as pushes vapor in a direction opposite to that of the incoming liquid. Hence, vapor accumulation along the heated wall and vapor removal along the flow channel are both highly dependent upon the magnitude of buoyancy force relative to liquid inertia.

Low velocity flows are particularly prone to both low CHF and complex flow interactions for downward flow and a downward-facing heated wall. Here, weak liquid inertia greatly magnifies the role of buoyancy forces. Very small velocity flows approach pool boiling conditions for which studies have demonstrated appreciable sensitivity of CHF to heated wall orientation [1–5]. Drastically different CHF mechanisms were identified for different orientation ranges relative to gravity. These mechanisms could be divided into three main orientation regions [5]. The classical description of CHF from a horizontal surface encompasses upward-facing heated wall orientations. Near-vertical orientations, on the other hand, produce a wavy vapor layer that is driven by buoyancy forces along the wall, mimicking flow boiling CHF. Downward-facing orientations produce very low CHF values resulting from stratification of a fairly continuous vapor layer beneath the heated wall.

Most studies on the effects of orientation on flow boiling concern the drastic differences in CHF between vertical upflow and vertical downflow. Simoneau and Simon [6] showed vapor motion in vertical downflow switches from concurrent at high liquid velocities to countercurrent at low velocities. CHF values for vertical downflow were lower than for vertical upflow at the same velocity, but differences between the two opposite orientations decreased with increasing liquid velocity. Mishima et al. [7] also measured smaller CHF for downflow than for upflow at the same velocity. They examined the delicate equilibrium between liquid inertia and buoyancy force for downflow, illustrating how this balance can bring about stagnation of vapor masses in the channel and unusually low CHF values. Gersey and Mudawar [8] confirmed the findings of Simoneau and Simon and Mishima et al.in a study of the effects of flow orientation on CHF in microprocessor cooling.

The primary objective of the present study is to (a) identify and explore CHF mechanisms associated with different flow boiling orientations, and (b) develop a systematic method for assessing the importance of body force on flow boiling CHF. High-speed video imaging is employed to capture vapor behavior at conditions just preceding the occurrence of CHF. These photographic studies yielded clear images of the vapor-liquid interface and helped track both the spatial and temporal behavior of the vapor-liquid interface. CHF data are compared to predictions of previous models and correlations in an assessment of the suitability of these tools to thermal design of boiling systems at different orientations and different flow velocities. Finally, this information is used to develop a new systematic theoretically-based method for assessing the significance of body force on flow boiling CHF.

Contributed by the Heat Transfer Division for publication in the JOURNAL OF HEAT TRANSFER. Manuscript received by the Heat Transfer Division June 3, 2003; revision received November 19, 2003. Associate Editor: M. K. Jensen.

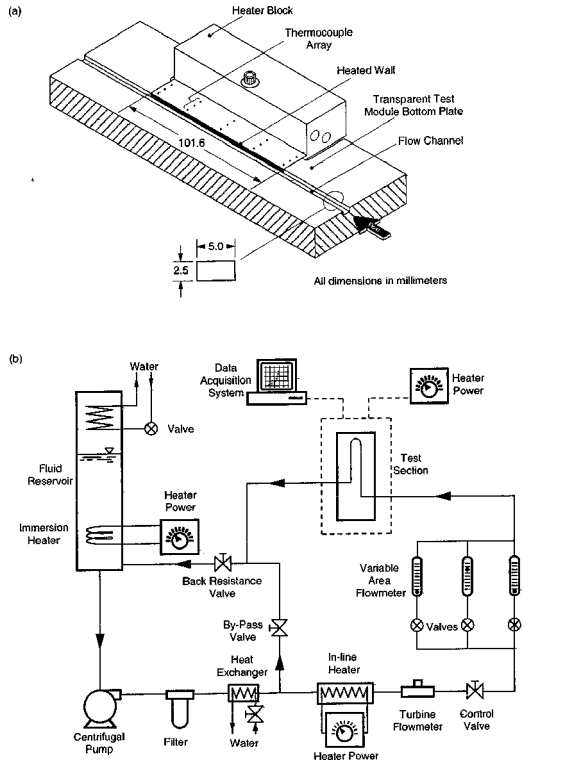

Fig. 1 (*a*) Heater inserted into bottom plate of test module; and (*b*) Two-phase flow loop

2 Experimental Method

2.1 Experimental Apparatus. The apparatus for this study featured a transparent test module which enabled side-viewing of vapor behavior along a heated wall. The module was formed by bolting together two plates of Lexan, a polycarbonate plastic which combines the attractive attributes of machinability, optical clarity and relatively high deflection temperature. A 5.0 $\times 2.5\ \mathrm{mm}^2$ rectangular flow channel was milled into the bottom plate of the test module. As shown in Fig. 1(*a*), the heated wall consisted of a thin edge of a copper heater which was inserted into the bottom plate, and carefully aligned with one side of the flow channel. Liquid FC-72 was introduced from a compression fitting leading to a small plenum that was fitted with a honeycomb flow straightener. An entry length 106 times the channel hydraulic diameter provided fully-developed flow upstream of the heated wall. Thermocouples were inserted into the flow channel both upstream and downstream of the heated wall. Similarly, pressure transducers were connected to pressure taps at about the same locations as the flow thermocouples. Output signals from these thermocouples and pressure transducers enabled continued monitoring of the changes in fluid state during the tests.

The heater was fabricated from a single block of pure copper. The heated wall measured 2.5 mm in width and 101.6 mm along the flow direction. Heat was supplied by four 150-W cartridge heaters that were embedded in the thick portion of the copper block. As shown in Fig. 1(*a*), five sets Type-K thermocouples, each consisting of three thermocouples, were inserted along the heater to determine axial variations of both wall flux and wall temperature. A linear fit to the three thermocouple readings was determined at each of the five thermocouple locations. This temperature profile was extrapolated to the wall to determine the wall temperature, T_w, while the heat flux, q'', was calculated from the temperature gradient. Table 1 summarizes the uncertainty estimates for the key measured and derived quantities of this study.

Fluid conditioning was accomplished with the aid of a compact two-phase loop illustrated schematically in Fig. 1(*b*). Fluid temperature was modulated by a water-cooled flat-plate heat exchanger followed by an in-line electrical immersion heater. The latter was controlled by a variable transformer to finely-tune liquid temperature at the inlet to the test module.

Table 1 Uncertainty estimates for key measured and derived quantities

Parameter	Symbol	Uncertainty
Thermocouples	-	$<0.3°C$
Pressure	P_o	$<0.01\%$
Velocity	U	$<2.3\%$
Heat Flux	q'', q''_m	$<7.9\%$
Temperature difference	$T_w - T_{in}$	$<0.9°C$

The working fluid used in this study, FC-72, is well suited for flow visualization of the CHF mechanism. Unlike water, whose CHF detection is sometimes accompanied by permanent damage to test module hardware, the low boiling point (56°C at atmospheric pressure) and low heat of vaporization of FC-72 produce relatively mild temperature excursions at CHF. This helps ensure reusability of the test module following repeated CHF tests, as well as provide ''ample'' time for photographic study of vapor behavior at CHF with less concern over the likelihood of test module physical burnout.

2.2 Photographic Techniques. A Redlake MotionScope PCI 8000s high-speed digital video system was used to capture vapor-liquid interfacial features just prior to CHF. The video camera in this system is capable of recording speeds from 60 to 8000 frames per second (fps) with 256 gray scale levels, and its electronic shutter can be modulated from $1/60^{\mathrm{th}}$ s down to 10 μs. Selecting an appropriate speed for the present study was based on several requirements, most important of which were lighting, resolution, and minimal interfacial shift. Optimum video imaging was realized with a recording rate of 1000 fps and a shutter speed of 50 μs. The system recorded over 2 s of video, which consisted of 2048 individual frames, each consisting of 240×210 pixels.

The video camera was positioned normal to the front of the flow channel. The high shutter speed adopted in this study demanded intense back lighting, which was made possible by a 0–2400 W light source that was separated from the channel by a diffuser plate. A high stability translation platform maneuvered the camera along the flow direction. Three different camera positions were used, which enabled video imaging of either the upstream, middle, or downstream sections of the heated wall. This paper provides sequential images of the downstream one-third of the heated wall where CHF is detected. The time interval between two successive images is 2 ms.

2.3 Operating Conditions and Test Procedure. Tests were conducted at eight different flow orientations as illustrated in Fig. 2. Each orientation is characterized by a specific flow direction relative to Earth's gravity, as well as orientation of the heated wall. The orientation $\theta = 0$ deg marks the horizontal flow orientation with the heated wall facing upwards. Other orientations, which were examined at 45 deg increments, produced horizontal flow, upflow or downflow, with the heated wall facing upwards or downwards.

Five inlet liquid velocities ($U = 0.1$, 0.2, 0.5, 1.0, and 1.5 m/s) were studied for each orientation. Since CHF occurred at the downstream thermocouple set, the CHF data were referenced to thermodynamic conditions at the heated wall exit. A constant outlet pressure of $P_o = 1.38$ bar (20 psia), corresponding to a saturation temperature of $T_{\mathrm{sat},o} = 66.3°C$, was maintained throughout the study. For each velocity, the inlet temperature was modulated to produce an outlet temperature of 63.3°C, corresponding to a 3°C outlet subcooling, when CHF occurred.

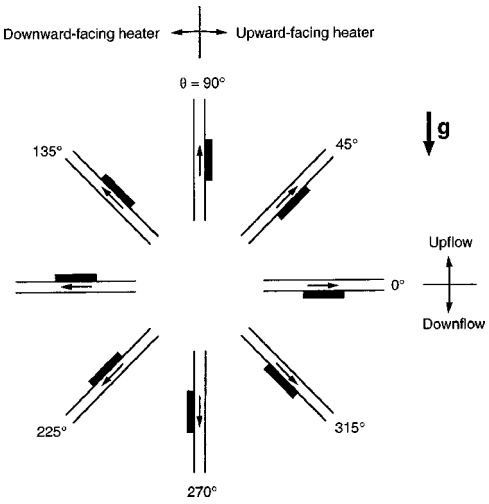

Fig. 2 Flow orientation guide indicating flow direction, channel orientation, and heater location (indicated by black rectangle)

A consistent operating procedure was adopted throughout the study. Each test commenced by controlling the various components of the flow loop to yield the desired inlet temperature, outlet pressure and flow rate. Heat was then supplied to the test module heater in increments of $1-3\ \mathrm{W/cm^2}$ (which were reduced as CHF was approached to refine CHF detection), and data were recorded once hydrodynamic and thermal conditions were deemed steady. Each test progressed through the single-phase and nucleate boiling regimes, generating a boiling curve, and was terminated immediately after CHF detection.

3 CHF Regimes

Figure 3(*a*) shows all CHF data collected from this study in a flow velocity-flow orientation plane. The CHF data are grouped into six different regimes for which representative photographs are depicted in Fig. 3(*b*). The most obvious feature of this CHF map is the existence of a dominant *Wavy Vapor Layer Regime* corresponding to all high velocities at all orientations. At and below 0.5 m/s, there exist a number of complex CHF regimes. Notice that the Wavy Vapor Layer Regime is prevalent even for low velocities for the vertical and near-vertical orientations, $\theta = 90$ and 135 deg, respectively. This regime is consistent with CHF depictions of flow boiling by Galloway and Mudawar [9,10].

A *Pool Boiling Regime* exists for low velocities, and $\theta = 0$, 45, and 315 deg. Bubble behavior within these horizontal and near-horizontal orientations with an upward-facing heated wall resembles pool boiling CHF from large horizontal surfaces. All four remaining CHF regimes are associated with downflow and downward-facing heated wall orientations at low velocities.

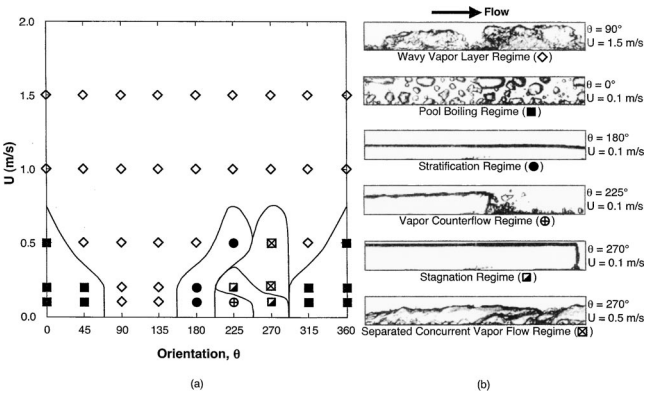

Fig. 3 (*a*) CHF regime map; and (*b*) Typical flow characteristics for each regime

The six CHF regimes are described below in terms of both the shape and temporal behavior of liquid-vapor interface. All the photographs discussed below correspond to the downstream one-third of the heated wall.

3.1 Wavy Vapor Layer Regime. As depicted in Fig. 3(*b*), this regime is characterized by large vapor patches that form along the heated wall, resembling a fairly continuous wavy vapor layer. This layer prevents liquid contact with much of the heated wall, producing broad regions of dry wall, except in wetting fronts, located in troughs between vapor patches, where virtually all the heat is dissipated. This regime was encountered at velocities of $U = 1.0$ and 1.5 m/s regardless of orientation and encompasses upflow orientations at lower velocities as well.

Figure 4(*a*) shows a series of seventeen sequential video images of conditions corresponding to the Wavy Vapor Layer Regime. These images were captured at 1000 fps, which allowed prominent vapor features to be carefully tracked with time. Clearly, the vapor patches and wetting fronts are not stationary, but propagate along the heated wall. The waviness associated with this CHF regime lends credence to the adoption of hydrodynamic instability theory is describing the vapor layer shape, amplitude, and propagation speed [9,10].

Figure 4(*a*) shows the liquid-vapor wavy interface is marred by smaller interfacial disturbances, apparently the result of increased turbulence intensity at high liquid velocities. Galloway and Mudawar [9,10] encountered the same Wavy Vapor Layer Regime in vertical upflow along a short heated wall. They too noticed that the wavy vapor layer interface became increasingly marred by small disturbances with increasing velocity.

3.2 Pool Boiling Regime. Figures 3(*a*) shows this regime encompasses velocities below 0.5 m/s with the heated wall facing upwards ($\theta = 315$, 0, and 45 deg). Figure 3(*b*) shows small bubbles coalescing into larger ones, which are detached by buoyancy and driven across the flow channel to the opposite wall, where the vapor accumulates into yet larger vapor masses.

Figure 4(*b*) shows sequential images of this regime corresponding to $\theta = 0°$ and $U = 0.1$ m/s. While the vapor masses seem to propagate along the heated wall, the speed of propagation is much smaller than in Fig. 4(*a*), corresponding to $\theta = 90$ deg and $U = 1.5$ m/s. The low liquid velocity in Fig. 4(*b*) produces very mild drag forces on the vapor features, evidenced both by the aforementioned low speed of propagation of vapor masses, as well as the relatively mild deformation in the shape of coalescent bubbles departing normal to the heated wall. This is the primary reason behind the authors' naming of this regime, which is dominated by buoyancy forces. However, even in this Pool Boiling Regime, increasing liquid velocity should help remove vapor along the flow channel and preclude merging of vapor masses between the heated wall and opposite wall.

3.3 Stratification Regime. The same low velocities that caused buoyancy to dominate vapor formation in the previous Pool Boiling Regime are responsible for the formation of a well separated vapor layer which stratifies against the heated wall for horizontal and near-horizontal downward-facing wall orientations, $\theta = 180$ and 225 deg, respectively. As shown in Fig. 3(*b*), this thick continuous vapor layer greatly impedes liquid access to the heated wall, resulting in very low CHF values.

The sequential video images of the stratified vapor layer in Fig. 4(*c*) show the vapor layer interface is somewhat wavy, but the wavelength is fairly long, exceeding the entire heated length, and has a very small amplitude. This behavior points to hydrodynamic conditions which promote a stable liquid-vapor interface. Such a stable interface is very detrimental to the heat transfer process. An

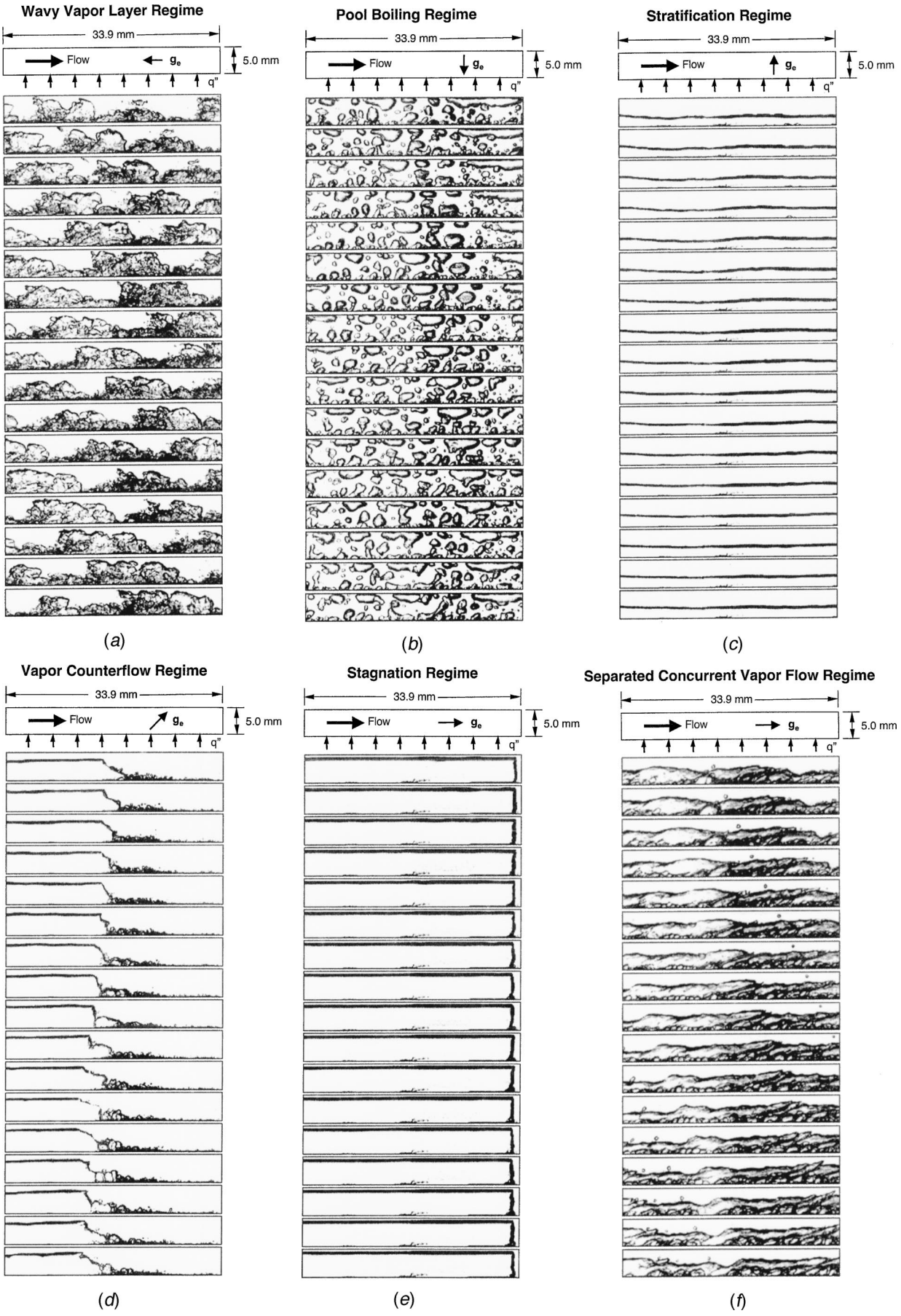

Fig. 4 Sequential images of vapor layer at (*a*) θ=90 deg and U=1.5 m/s, (*b*) θ=0° and U=0.1 m/s, (*c*) θ=180 deg and U=0.1 m/s, (*d*) θ=225 deg and U=0.1 m/s, (*e*) θ=270 deg and U=0.1 m/s, and (*f*) θ=270 deg and U=0.5 m/s

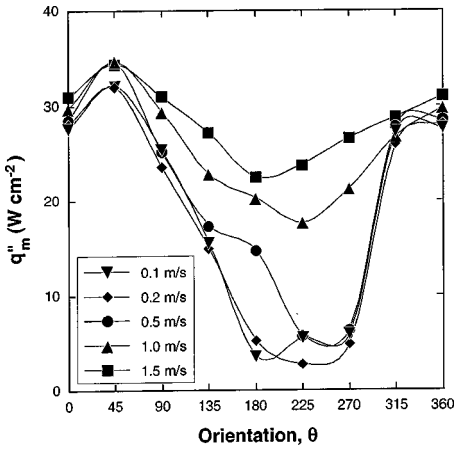

Fig. 5 CHF variation with orientation and flow velocity

unstable interface, on the other hand, causes both spatial and temporal growth of interfacial amplitude, permitting liquid access to the heated wall.

3.4 Vapor Counterflow Regime. This regime as well as the two remaining CHF regimes discussed below are closely related to the relative magnitude of liquid inertia and buoyancy force for downflow orientations at low velocities. As shown in Fig. 3(*a*), the Vapor Counterflow Regime was encountered at $\theta=225$ deg for $U=0.1$ m/s. At this low velocity, the liquid drag force exerted downwards upon the vapor is far too weak to overcome the opposing buoyancy force. The later pushes vapor backwards (upwards) against the incoming liquid. The sequential images in Fig. 4(*d*) show the thick coalescent vapor layer moving backwards, albeit very slowly, as liquid continues to make contact over the downstream portion of the heated wall.

3.5 Stagnation Regime. This regime was encountered when the liquid drag force and inertia came into balance, effectively freezing a thick coalescent vapor mass in place. As shown in Fig. 3(*a*), this condition occurs at $\theta=225$ deg for $U=0.2$ m/s and $\theta=270$ deg for $U=0.1$ m/s. Figure 3(*b*) and the sequential images in Fig. 4(*e*) show liquid contact with the downstream section of the heated wall is available over of a very small region. The sequential images show the thick, continuous vapor layer is virtually stationary. This behavior produced the lowest CHF values of the present study. In fact, at $\theta=225$ deg, CHF at 0.1 m/s (corresponding to the Vapor Counterflow Regime) was actually greater than CHF at the higher velocity of 0.2 m/s corresponding to the Stagnation Regime.

3.6 Separated Concurrent Vapor Flow. The stagnant vapor layer described in the previous section was purged from the channel with an increase in inlet liquid velocity that allowed the liquid drag force to overcome buoyancy. Figure 3(*a*) shows this regime is encountered at $\theta=270$ deg for $U=0.2$ and 0.5 m/s. This regime is complicated by significant disturbances along the vapor-liquid interface and bubble formation in a thin liquid layer at the heated wall which is, for the most, separated from the bulk liquid flow. The sequential images in Fig. 4(*f*) show the vapor layer interface propagating with a large wavelength and small amplitude along the channel. Figure 3(*a*) shows increasing liquid velocity at this orientation from 0.5 to 1.0 m/s causes the vapor layer interface to become unstable, marking a transition to the Wavy Vapor Layer Regime described before.

4 CHF Results

Figure 5 shows the variation of CHF with orientation for the five velocities tested. As indicated before, all these data are referenced to thermodynamic conditions based on the heated wall exit: $P_o=1.38$ bar, $T_{\text{sat},o}=66.3$ deg C, and 3 deg C outlet subcooling. For all velocities, CHF increases from $\theta=0$ deg to a maximum around 45 deg, followed by a decrease to a minimum between 180 and 270 deg, before recovering again to the $\theta=0°$ value. The three lowest velocities of $U=0.1$, 0.2, and 0.5 m/s exhibit strong variations of CHF with orientation. These velocities produce very small CHF values in the range of $180<\theta<270$ deg. This further demonstrates the significance of buoyancy force compared to liquid inertia at low flow velocities. As illustrated in Figs. 3(*b*) and 4(*c–f*), the relatively weak liquid inertia enables buoyancy to dominate vapor behavior, causing vapor stratification against the heated wall for $\theta=180$ deg, and inducing Vapor Counterflow, Stagnation, or Separated Vapor Concurrent Flow for $\theta=225$ and 270 deg. Clearly, downflow and downward-facing heated wall orientations should be avoided at low velocities.

Figure 5 shows the two highest velocities, 1.0 and 1.5 m/s, cause appreciable diminution in the orientation effects on CHF. Nonetheless, buoyancy still influences CHF at these two velocities. A CHF maximum at $\theta=45$ deg can be explained by the buoyancy force both aiding vapor removal away from the heated wall as well as along the channel. At $\theta=0$ deg, buoyancy is perpendicular to the heated wall but does not aid the vapor removal along the channel, while the opposite is true for $\theta=90$ deg. CHF for $U=1.0$ and 1.5 m/s decreases for all downflow and downward-facing heated wall orientations, but to a much lesser degree than for the lower velocities.

Since the Wavy Vapor Layer Regime was observed for a large fraction of the present operating conditions, it is prudent to explore the dependence of interfacial instability on the forces which influence vapor behavior at different velocities and orientations. The speed of an idealized sinusoidal liquid-vapor interface between a vapor layer moving at velocity U_g and a liquid layer at U_f can be expressed as [10]

$$c=\frac{\rho_f U_f+\rho_g U_g}{\rho_f+\rho_g} \pm \sqrt{\frac{\sigma k}{\rho_f+\rho_g}-\frac{\rho_f\rho_g(U_g-U_f)^2}{(\rho_f+\rho_g)^2}-\frac{(\rho_f-\rho_g)}{(\rho_f+\rho_g)}\frac{g_e\cos\theta}{k}} \quad (1)$$

where k is the wave number. A negative argument in the radical of Eq. (1) results in a wave speed containing both real and imaginary components. The imaginary component

$$c_i=\sqrt{\frac{\rho_f\rho_g(U_g-U_f)^2}{(\rho_f+\rho_g)^2}+\frac{(\rho_f-\rho_g)}{(\rho_f+\rho_g)}\frac{g_e\cos\theta}{k}-\frac{\sigma k}{\rho_f+\rho_g}} \quad (2)$$

represents the combined effect of the different forces and dictates the stability (or instability) of the interface. The first term under the radical in Eq. (2) is a measure of the destabilizing effect of inertia, or velocity difference between the vapor and liquid phases. The second term is the body force effect, which, for a terrestrial environment, may be stabilizing or destabilizing depending on orientation of the wall relative to gravity. The third term accounts for surface tension which is always stabilizing to the interface.

The critical wavelength, defined as the wavelength of a neutrally stable wave, can be determined by setting the radical in Eq. (2) equal to zero.

$$\frac{2\pi}{\lambda_c}=\frac{\rho_f\rho_g(U_g-U_f)^2}{2\sigma(\rho_f+\rho_g)} + \sqrt{\left[\frac{\rho_f\rho_g(U_g-U_f)^2}{2\sigma(\rho_f+\rho_g)}\right]^2+\frac{(\rho_f-\rho_g)g_e\cos\theta}{\sigma}}. \quad (3)$$

Figure 6 shows CHF data for the limiting velocities of 0.1 and 1.5 m/s versus orientation angle. Also shown are predictions based on previous semi-empirical and theoretical CHF models. The Interfacial Lift-off Model, first proposed by Galloway and Mudawar [9,10] in the early 1990s, is intended for the dominant Wavy Vapor Layer Regime depicted in Figs. 3(*b*) and 4(*a*). This model is based on the assumption that the wavy layer makes contact with

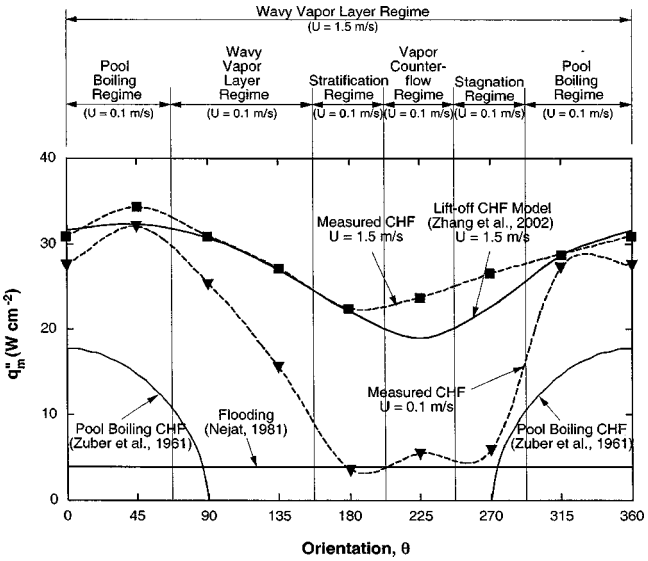

Fig. 6 Comparison of CHF data for lowest and highest velocities with predictions based on previous models and correlations for 5 mm×2.5 mm rectangular channel and operating conditions of present study

the heated wall over relatively short discrete regions corresponding to the wave troughs. It postulates that CHF will occur when the intense momentum of vapor generated normal to the wall exceeds the pressure force resulting from the interfacial curvature. Recently, the authors of the present study modified this model to explore the effects of orientation and interfacial wave growth [11]. Their model predictions show good agreement with the 1.5 m/s data as shown in Fig. 6. Convergence was never achieved with this model for $U=0.1$ m/s because of the large critical wavelength. Data for this lower velocity are compared to predictions of the classical CHF model of Zuber et al. [12] for pool boiling from a horizontal upward-facing heated wall. The gravitational acceleration, g_e, in the original model was replaced by $g_e \cos\theta$ since the Taylor instability employed in the model is based on only the component of gravity perpendicular to the heated wall.

$$q''_m = 0.131 \rho_g h_{fg} \left[\frac{\sigma(\rho_f - \rho_g) g_e \cos\theta}{\rho_g^2} \right]^{1/4}. \tag{4}$$

Figure 6 shows the pool boiling CHF model underpredicts CHF data corresponding to the present Pool Boiling Regime because it does not incorporate the benefits of liquid motion and its contribution to vapor removal along the channel.

Also shown in Fig. 6 are CHF predictions based on Negat's [13] flooding criterion

$$q''_m = 0.36 \left(\frac{L}{D_h} \right)^{0.1} \left(\frac{A}{A_w} \right) \rho_g h_{fg} \left[\frac{(\rho_f - \rho_g) g_e D_h}{\rho_g} \right]^{1/2} \left[1 + \left(\frac{\rho_g}{\rho_f} \right)^{1/4} \right]^{-2}, \tag{5}$$

which was derived for a closed-end vertical heated tube, where L, D_h, A, and A_w are the heated length, hydraulic diameter, heated area, and channel cross-sectional area, respectively. Figure 6 shows all 0.1 m/s CHF data belonging to the Stratification, Vapor Counterflow, and Stagnation Regimes approach the flooding limit. This limit occurs when vapor upflow in a pipe with a closed bottom prevents liquid from flowing downwards to replenish liquid that has been evaporated. This situation resembles the vapor behavior observed in this study in conjunction with the Vapor Counterflow and Stagnation Regimes, but not the Stratification Regime.

Figure 6 proves the Interfacial Lift-off Model is an effective tool for predicting high velocity flow boiling CHF for all orientations, while the flooding limit is useful for estimating CHF at low velocities and downflow orientations. However, a more systematic and comprehensive methodology is needed to design thermal management systems that can overcome the effects of body force on flow boiling CHF for different fluids and gravitational fields. Aside for terrestrial applications, such a tool is highly desired for design of thermal management hardware in space applications.

5 Methodology for Overcoming Body Force on Flow Boiling CHF

Flow orientation is sometimes dictated by system considerations other than heat dissipation. As indicated before, body force influences flow boiling CHF in the following three ways:

1. The body force component that is perpendicular to the heated wall influences hydrodynamic instability of the vapor-liquid interface.
2. The body force component in the direction of (or opposite to) the liquid flow influences vapor removal from the channel and may trigger flooding at low velocities.
3. A very long critical wavelength may preclude liquid contact with a large fraction of the heated wall.

Therefore, three separate criteria must be developed to overcome the effects of body force on flow boiling CHF.

5.1 Effects of Component of Body Force Perpendicular to Heated Wall. Equation (2) reveals interfacial instability of a vapor-liquid interface in a flow channel is governed by the combined effect of inertia, surface tension, and component of body force that is perpendicular to the heated wall. Equation (3) can be rearranged in the following form:

$$\frac{2\pi}{\lambda_c} \frac{\sigma(\rho_f + \rho_g)}{\rho_f \rho_g (U_g - U_f)^2} = \frac{1}{2} \left\{ 1 + \sqrt{1 + 4 \frac{(\rho_f - \rho_g)(\rho_f + \rho_g)^2 \sigma g_e \cos\theta}{\rho_f^2 \rho_g^2 (U_g - U_f)^4}} \right\} \tag{6}$$

The right-hand-side of Eq. (6) approaches unity when the component of body force perpendicular to the heated wall is too weak to influence interfacial instability. This constitutes a sufficient condition for negating the influence of this component of body force on CHF and which corresponds to flows that fall into the Wavy Vapor Layer Regime. This condition can be expressed as

$$\left| \frac{(\rho_f - \rho_g)(\rho_f + \rho_g)^2 \sigma g_e \cos\theta}{\rho_f^2 \rho_g^2 (U_g - U_f)^4} \right| \ll \frac{1}{4}. \tag{7}$$

This criterion was examined by substituting the phase velocity difference by the characteristic velocity of the flow channel, namely U. The left-hand-side of Eq. (7) can also be expressed as $\mathrm{Bo/We}^2$, where Bo and We are the Bond and Weber numbers, respectively, which are defined as

$$\mathrm{We} = \frac{\rho_f \rho_g U^2 L}{(\rho_f + \rho_g)\sigma} \tag{8}$$

and

$$\mathrm{Bo} = \frac{(\rho_f - \rho_g) g_e \cos\theta L^2}{\sigma}. \tag{9}$$

Figures 7(*a*) and 7(*b*) show the variation of $\mathrm{Bo/We}^2$ with orientation and flow velocity. The peak values of $\mathrm{Bo/We}^2$ for $U=0.1$, 0.2, 0.5, 1.0 and 1.5 m/s are 4503, 281, 7.2, 0.45, and 0.09, respectively. The large values corresponding to $U=0.1$ and 0.2 m/s are consistent with the strong influence of orientation on CHF for these velocities. Conversely, the small values of $\mathrm{Bo/We}^2$ for $U=1.0$ and 1.5 m/s are indicative of a very weak influence of body force on CHF for these velocities, as was clearly demonstrated in the flow boiling experiments. Since the CHF data

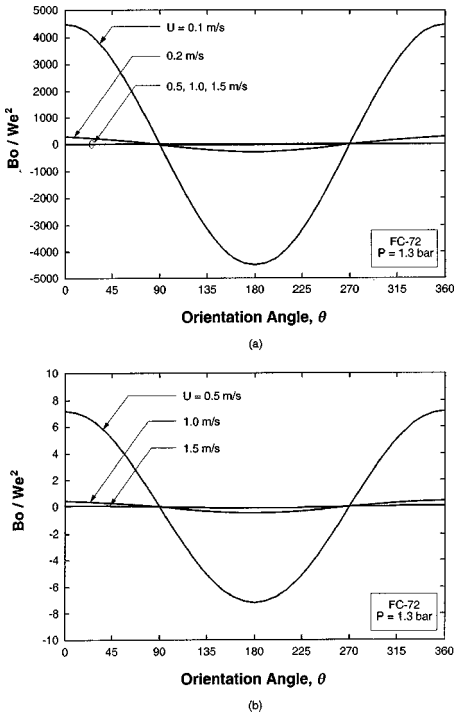

Fig. 7 Variation of Bo/We^2 with flow orientation and velocity for (*a*) all velocities tested and (*b*) $U \geqslant 0.5$ m/s

showed little dependence on orientation for $U \sim 1.5$ m/s, the magnitude of Bo/We^2 for $U=1.5$ m/s is used as a criterion for overcoming body force effects on CHF.

$$\frac{\mathrm{Bo}}{\mathrm{We}^2} = \frac{(\rho_f - \rho_g)(\rho_f + \rho_g)^2 \sigma g_e}{\rho_f^2 \rho_g^2 U^4} \leqslant 0.09. \tag{10}$$

5.2 Effects of Component of Body Force Parallel to Heated Wall. Several complex CHF regimes were identified in the present study for predominantly downflow orientations at low velocities. The Vapor Counterflow and Vapor Stagnation CHF regimes were both the result of the relative velocity between the vapor and liquid phases, while the Separated Concurrent Vapor Flow was a transitional regime between the Vapor Stagnation and Wavy Vapor Layer CHF regimes. In the Vapor Stagnation and Vapor Counterflow Regimes, the vapor took the form of a long slug bubble as shown in Fig. 4(*e*). The rise velocity of a slug bubble relative to liquid can be expressed as [14]

$$U_\infty = 0.35 \frac{[(\rho_f - \rho_g) g_e \sin\theta \ D_h]^{1/2}}{\rho_f^{1/2}} \tag{11}$$

When U_∞ exceeds the liquid velocity, U, the vapor tends to flow backwards relative to the liquid. Vapor Stagnation occurs when the two velocities are equal. A sufficient condition for negating vapor counterflow and vapor stagnation is $U_\infty \ll U$, which, for $\sin\theta = 1$, can be represented in terms of the Froude number,

$$\frac{1}{\mathrm{Fr}} = \left| \frac{(\rho_f - \rho_g) g_e \sin\theta \ D_h}{\rho_f U^2} \right| \ll 8.16. \tag{12}$$

Figures 8(*a*) and 8(*b*) show the variation of 1/Fr for different orientations and flow velocities. For $U=0.1$ and 0.2 m/s and $\theta = 225$ and 270 deg, where vapor counterflow and vapor stagnation were observed, Fig. 8(*a*) shows the magnitude of 1/Fr is larger than 0.82. Conversely, Fig. 8(*b*) shows the magnitude of 1/Fr for the other higher velocities is less than 0.13. Since vapor counterflow and vapor stagnation where not observed for $U=0.5$ m/s, a

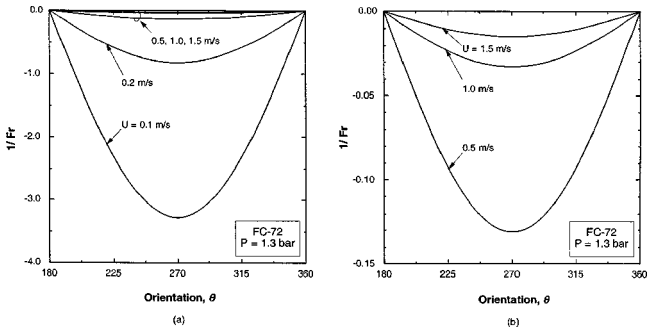

Fig. 8 Variation of 1/Fr with flow orientation and velocity for (*a*) all velocities tested and (*b*) $U \geqslant 0.5$ m/s

sufficient criterion for precluding the occurrence of these flow anomalies can be expressed for $\sin\theta = 1$ by the criterion

$$\frac{1}{\mathrm{Fr}} = \frac{(\rho_f - \rho_g) g_e D_h}{\rho_f U^2} \leqslant 0.13 \tag{13}$$

5.3 Critical Wavelength Versus Heated Length. As discussed before, low flow velocities can produce very large values of critical wavelength. Replacing the phase velocity difference by the characteristic velocity of the flow channel, Eq. (6) reveals the largest value of critical wavelength is given by

$$\lambda_c = \frac{2\pi\sigma(\rho_f + \rho_g)}{\rho_f \rho_g U^2}. \tag{14}$$

Thus, to maintain a critical wavelength shorter than the heated length, L, the following Weber number criterion must be satisfied:

$$\mathrm{We} = \frac{\rho_f \rho_g U^2 L}{(\rho_f + \rho_g)\sigma} \geqslant 2\pi. \tag{15}$$

5.4 Minimum Flow Velocity Required to Overcome Body Force Effects. It is now possible to combine the above three criteria in pursuit of a comprehensive methodology to overcome body force effects. Equations (10), (13), and (15) reveal that increasing flow velocity is perhaps the most effective means for satisfying these criteria. Velocity is an important parameter for the design of thermal management systems in both terrestrial and space applications. For the latter, coolant velocity has a strong bearing on pumping power and therefore overall power consumption. Using low velocities is therefore vital to reducing power consumption provided the aforementioned flow anomalies can be prevented.

Figure 9 shows the minimum velocity required to satisfy the above criteria as a function of a/g_e, the ratio of body force per unit mass to Earth's gravity. This was accomplished by substituting g_e in Eqs. (10) and (13) by a. Avoiding body force effects requires that flow velocity exceed values predicted by each of the three criteria. Only one of these criteria is dominant for a given value of a/g_e. Figure 9 shows fairly appreciable flow velocities will be required to overcome flooding effects, should a large body force of $a/g_e > 75$ be present in a direction opposite to the liquid flow. Instability effects are dominant when a body force of $a/g_e < 75$ is present in a direction perpendicular to the heated wall, as surface tension effects become increasingly important. These instability effects span Earth, Lunar and Martian environments. The heater length criterion is dominant for relatively low values of a/g_e. However, the transition a/g_e value between the instability-dominated and heater-length-dominated regimes is a function of the heated length; shorter heaters require higher velocities to decrease critical wavelength below the heated length. Overall, the heater-length-dominated regime appears quite significant for microgravity conditions.

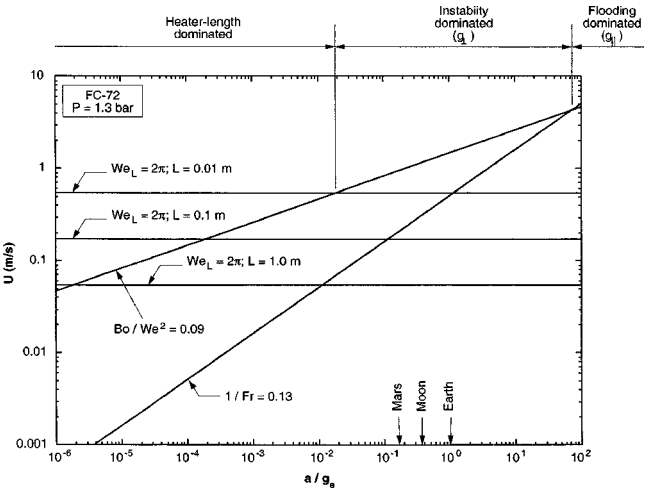

Fig. 9 Determination of minimum flow velocity required to overcome all body force effects on flow boiling CHF

Obviously, the validation of this methodology for determining the minimum velocity required to overcome body force effects on flow boiling CHF will require future tests with other coolants, especially in a reduced gravity environment. Such tests represent future goals for a follow-up study.

6 Conclusions

This study examined the complex interactions between liquid inertia and buoyancy force in flow boiling at different orientations. High-speed video imaging provided representative images of the vapor-liquid interface for different operating conditions and helped track both the spatial and temporal characteristics of the interface. Heat transfer measurements complemented the photographic study by providing a database for assessment of previous CHF models and correlations. Finally, a systematic methodology was developed to determine the minimum liquid velocity required to overcome the effects of body force on CHF. Key findings from this study are as follows:

1. Six different CHF regimes were identified: Wavy Vapor Layer, Pool Boiling, Stratification, Vapor Counterflow, Vapor Stagnation, and Separated Concurrent Vapor Flow. CHF is very sensitive to orientation for flow velocities below 0.2 m/s, where extremely low CHF values are measured, especially with downward-facing heated wall and downflow orientations. High flow velocities dampen the effects of orientation considerably. The Interfacial Lift-off Model is very effective at predicting CHF for high velocities at all orientations. The flooding limit, on the other hand, is useful at estimating CHF at low velocities and for downflow orientations.

2. Three dimensionless criteria were developed to determine the minimum flow velocity required to overcome body force effects on flow boiling CHF. Only one of the three criteria is dominant for a given gravitational field. This methodology may help reduce electric power consumption in space thermal management systems, provided it is ultimately validated for other coolants, especially in microgravity.

Acknowledgment

The authors are grateful for the support of the National Aeronautics and Space Administration under Grant No. NAG3-2336.

Nomenclature

a = body force per unit fluid mass
A = channel cross-sectional area
A_w = heated area of channel
Bo = bond number
c = wave speed
c_i = imaginary component of wave speed
D_h = channel hydraulic diameter
Fr = Froude number
g_e = earth's gravitational acceleration
$g_\perp$ = acceleration in flow direction
$g_\parallel$ = acceleration perpendicular to heated wall
h_{fg} = latent heat of vaporization
k = wave number
L = heater length in flow direction
P_o = outlet pressure
q'' = wall heat flux
q''_m = critical heat flux
$T_{\mathrm{sat},o}$ = saturation temperature based on measured outlet pressure
T_{in} = mean inlet liquid temperature
T_w = wall temperature
U = mean inlet liquid velocity
ΔU = velocity difference between vapor and liquid layers
U_f = velocity of liquid layer
U_g = velocity of vapor layer
U_∞ = rise velocity of slug bubble
We = Weber number

Greek Symbols

θ = flow orientation angle
λ_c = critical wavelength
ρ_f = density of saturated liquid
ρ_g = density of saturated vapor
σ = surface tension

References

[1] Class, C. R., DeHaan, J. R., Piccone, M., and Cost, R. B., 1960, "Boiling Heat Transfer to Liquid Hydrogen from Flat Surfaces," *Advances in Cryogenic Engineering*, K. D. Timmerhaus, ed., Plenum Press, New York, **5**, pp. 254–261.
[2] Marcus, W. R., and Dropkin, D., 1963, "The Effect of Surface Configuration on Nucleate Boiling Heat Transfer," Int. J. Heat Mass Transfer, **6**, pp. 863–867.
[3] Nishikawa, K., Fujita, Y., Uchida, S., and Ohta, H., 1983, "Effect of Heating Surface Orientation on Nucleate Boiling Heat Transfer," *Proc. ASME-JSME Thermal Engineering Joint Conference*, Y. Mori and W. J. Yang, eds., Honolulu, HI, **1**, pp. 129–136.
[4] Mudawar, I., Howard, A. H., and Gersey, C. O., 1997, "An Analytical Model for Near-Saturated Pool Boiling CHF on Vertical Surfaces," Int. J. Heat Mass Transfer, **40**, pp. 2327–2339.
[5] Howard, A. H., and Mudawar, I., 1999, "Orientation Effects on Pool Boiling CHF and Modeling of CHF for Near-Vertical Surfaces," Int. J. Heat Mass Transfer, **42**, pp. 1665–1688.
[6] Simoneau, R. J., and Simon, F. F., 1966, "A Visual Study of Velocity and Buoyancy Effects on Boiling Nitrogen," NASA Tech Note TN D-3354.
[7] Mishima, K., Nishihara, H., and Michiyoshi, I., 1985, "Boiling Burnout and Flow Instabilities for Water Flowing in a Round Tube under Atmospheric Pressure," Int. J. Heat Mass Transfer, **28**, pp. 1115–1129.
[8] Gersey, C. O., and Mudawar, I., 1993, "Orientation Effects on Critical Heat Flux from Discrete, In-Line Heat Sources in a Flow Channel," ASME J. Heat Transfer, **115**, pp. 973–985.
[9] Galloway, J. E., and Mudawar, I., 1993, "CHF Mechanism in Flow Boiling from a Short Heated Wall-Part 1. Examination of Near-Wall Conditions with the Aid of Photomicrography and High-Speed Video Imaging," Int. J. Heat Mass Transfer, **36**, pp. 2511–2526.
[10] Galloway, J. E., and Mudawar, I., 1993, "CHF Mechanism in Flow Boiling from a Short Heated Wall-Part 2. Theoretical CHF Model," Int. J. Heat Mass Transfer, **36**, pp. 2527–2540.
[11] Zhang, H., Mudawar, I., and Hassan, M. M., 2002, "Experimental and Theoretical Study of Orientation Effects on Flow Boiling CHF," Int. J. Heat Mass Transfer, **45**, pp. 4463–4478.
[12] Zuber, N., Tribus, M., and Westwater, J. W., "The Hydrodynamic Crisis in Pool Boiling of Saturated and Subcooled Liquids," *Int. Dev. Heat Transfer: Proc. Int. Heat Transfer Conf.*, Boulder, CO, 1961, pp. 230–236.
[13] Nejat, Z., 1981, "Effect of Density Ratio on Critical Heat Flux in Closed End Vertical Tubes," Int. J. Multiphase Flow, **7**, pp. 321–327.
[14] Wallis, G. B., 1969, *One-Dimensional Two-Phase Flow*, New York, McGraw-Hill Book Company.